doi:10.1038/nature11306

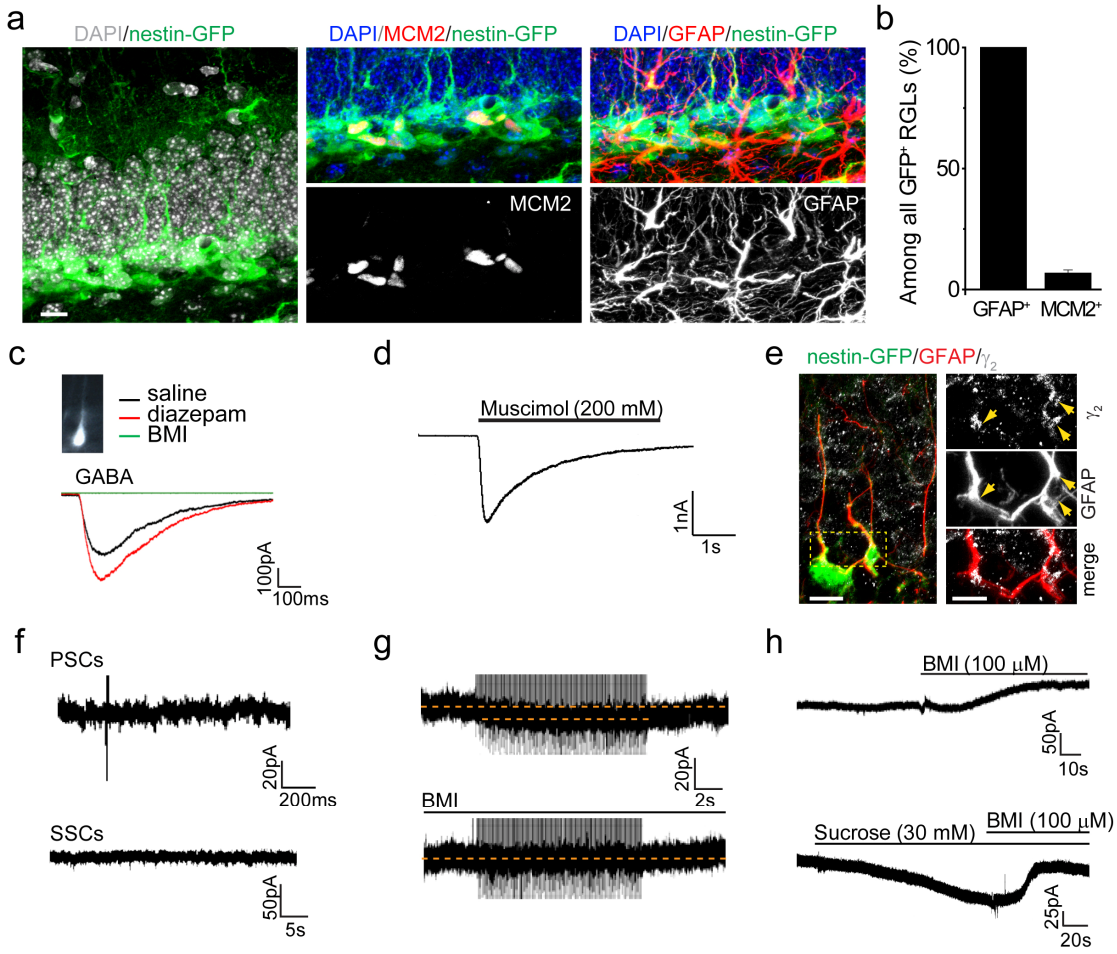

Supplementary Figure 1. Basic characterization of GFP$^+$ RGLs in the dentate gyrus of adult *nestin-GFP* mice. a, Sample confocal images of GFP, DAPI and immunostaining of GFAP and MCM2 in the dentate gyrus of adult *nestin-GFP* mice. Scale bar: 10 μm. **b**, Quantification of the percentages of GFAP$^+$ or MCM2$^+$ RGLs among all GFP$^+$ RGLs in the dentate gyrus of adult *nestin-GFP* mice. Values represent mean ± s.e.m. (n = 3 animals). **c-h**, Sample traces of whole-cell voltage-clamp recording from GFP$^+$ RGLs in slices acutely prepared from adult *nestin-GFP* mice (V_m = -65 mV). Shown are sample traces of a GFP$^+$ RGL in response to puffs of GABA (200 mM), in the presence or absence of diazepam (1 μM) or bicuculline (BMI; 50 μM, **c**), and response to muscimol (200 mM, **d**). Also shown is an imaging of a recorded cell loaded with dye through the recording pipette (**c**). Shown in (**e**) are sample confocal images of GFP$^+$ cells (green) immunostained for GFAP (red) and γ_2 (white) in the dentate gyrus of adult *nestin-GFP* mice. Scale bars: 10 μm (left) and 5 μm (right for insert). Shown in (**f**) are traces indicating a lack of evoked postsynaptic currents (PSCs) in a GFP$^+$ RGL in response to the field stimulation of the dentate granule cell layer (top) and no spontaneous synaptic currents (SSCs; bottom). Shown in (**g**) are sample traces of a GFP$^+$ RGL in response to a train of field stimuli (8 Hz, 100 stimuli) of the dentate granule cell layer, in the presence or absence of BMI (50 μM). Note tonic responses induced by the stimuli. Shown in (**h**) are sample traces from a GFP$^+$ RGL in response to bath application of bicuculline (BMI; 100 μM; top), revealing the basal level of tonic responses, and from a GFP$^+$ RGL in response to bath application of sucrose (30 mM) to increase the presynaptic release probability, followed by BMI treatment (bottom), demonstrating the presence of a tonic response to ambient GABA, but not synaptic GABAergic responses.

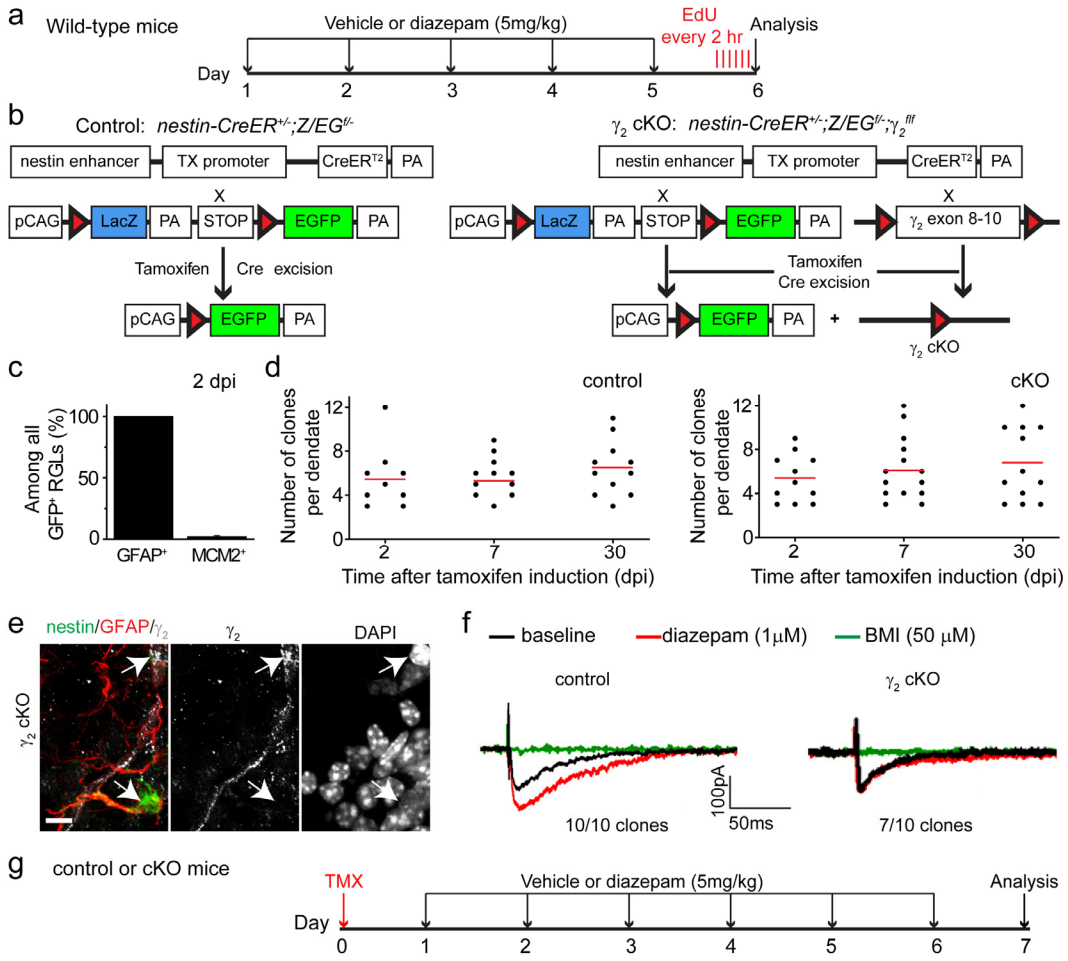

Supplementary Figure 2. Analysis of the role of γ_2-containing GABA$_A$Rs in regulating RGLs in the adult dentate gyrus. a, Experimental scheme for diazepam experiment (related to **Fig. 2a-b**). Wild-type adult mice were i.p. injected with diazepam (5 mg/kg body weight; once daily for 5 days), followed by 6 injections of EdU (41.1 mg/kg body weight) at 2 hrs apart, and then processed for immunohistology 2 hrs after the last EdU injection. **b**, A schematic diagram for *in vivo* clonal analysis of individual RGLs with or without conditional γ_2 deletion. **c-d**, Basic characterization of the clonal analysis approach. Shown in (**c**) is the quantification of immunohistological characterization of GFP$^+$ RGLs in the subgranular zone of the adult dentate gyrus of control mice at 2 dpi. Values represent mean ± s.e.m (n = 4-8 animals). Shown in (**d**) are total numbers of clones in each of the dentate gyrus examined for both control and γ_2 cKO adult mice under basal conditions. Each dot represents data from one dentate gyrus. Red lines represent mean values. **e-f**, Characterization of the efficacy of γ_2 deletion in the clonal analysis. Shown in (**e**) are sample confocal images of immunostaining of GFP, GFAP and γ_2. Scale bar: 10 μm. Shown in (**f**) are representative whole-cell recording traces of GABAergic synaptic currents from GFP$^+$ neurons before and after application of diazepam (1 μM) and BMI (50 μM) at 30 dpi in acute slices prepared from induced control and cKO mice. Numbers indicate number of clones with the phenotype among all recorded clones. **g**, A schematic diagram of experimental scheme to analyze the effect of systemic diazepam application in clonal analysis (related to **Fig. 2e & 3d**). After a single dose of tamoxifen injection (62 mg/kg body weight), vehicle or diazepam (5 mg/kg body weight) was *i.p.* injected once daily for 6 days, and animals were processed for immunohistology one day later for clonal analysis.

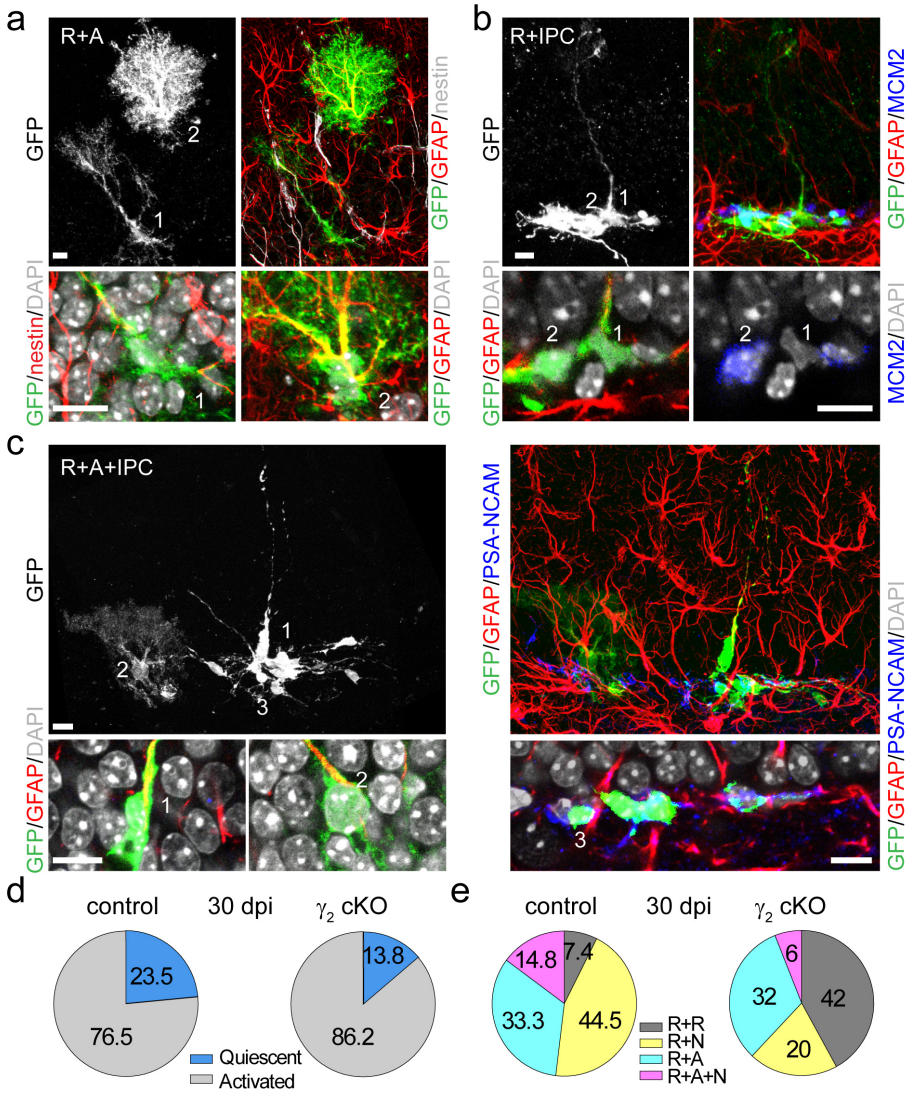

Supplementary Figure 3. Clonal analysis of γ_2 function in regulating RGLs at 30 dpi in the adult dentate gyrus. a-c, Sample confocal images of clones exhibiting active self-renewal. Shown in (**a**) is a GFP$^+$ clone consisting of a nestin$^+$GFAP$^+$ RGL (1) and a nestin$^-$GFAP$^+$ bushy astrocyte (2), indicating self-renewal and unipotential astrogenic differentiation. Shown in (**b**) is a GFP$^+$ clone consisting of a GFAP$^+$MCM2$^-$ RGL (1) and GFAP$^-$MCM2$^+$ IPCs (2), indicating self-renewal and unipotential neurogenic differentiation. Shown in (**c**) is a GFP$^+$ clone consisting of a GFAP$^+$ RGL (1), a GFAP$^+$ bushy astrocyte (2), and a cluster of cells of the neuronal lineage (3), some of which expressed immature neuronal marker PSA-NCAM, indicating self-renewal and multi-lineage differentiation. Scale bars: 10 μm. **d-e**, Quantitative comparison of the frequency of different clone types between control (n = 7) and γ_2 cKO (n = 6) at 30 dpi. Shown are pie charts of the relative frequency of quiescence/activation (**d**) and the summary of the frequency of different types among all RGL-containing GFP$^+$ clones (**e**).

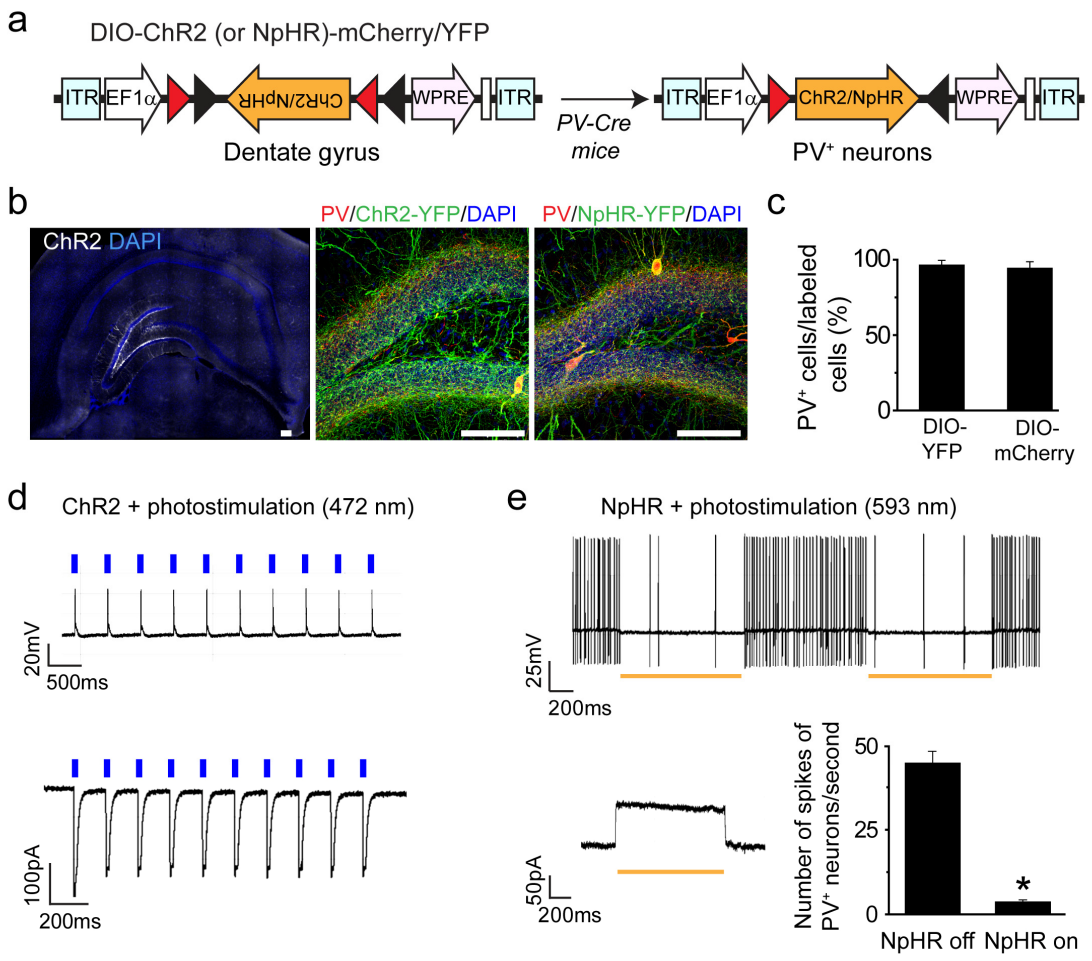

Supplementary Figure 4. Characterization of optogenetic tools for manipulating PV$^+$ interneuron activity in the adult dentate gyrus. a, A schematic diagram of AAV constructs used for Cre-dependent expression of ChR2 or eNpHR in PV$^+$ interneurons using adult *PV-Cre* mice. **b**, Sample confocal images of expression of ChR2-YFP or eNpHR-YFP and PV immunostaining 2 weeks after AAV-DIO-ChR2-YFP or AAV-DIO-NpHR-YFP injection into the dentate gyrus of adult *PV-Cre* transgenic mice. Scale bars: 50 μm. **c**, Quantification of the specificity of AAV-mediated expression in PV$^+$ interneurons in the adult dentate gyrus. Shown are summaries for both YFP and mCherry tagged opsin vectors (n = 5-10 animals). **d-e**, Effective photo-activation or suppression of PV$^+$ interneurons in slices acutely prepared from AAV injected animals. Shown are sample traces of whole-cell recordings of YFP$^+$PV$^+$ interneurons under both current-clamp (upper traces) and voltage-clamp modes (lower traces) upon photo-activation (**d**; 472 nm blue light at 8 Hz, 5 ms) or upon photo-suppression (**e**; 593 nm yellow light; constant). Also shown is the quantification of the efficiency of photo-induced suppression. A current pulse of 100 pA current was delivered to YFP$^+$PV$^+$ interneurons, and the number of action potentials with or without yellow light on was quantified. Values represent mean ± s.e.m. (n = 6 cells; *: $P < 0.05$; student t-test).

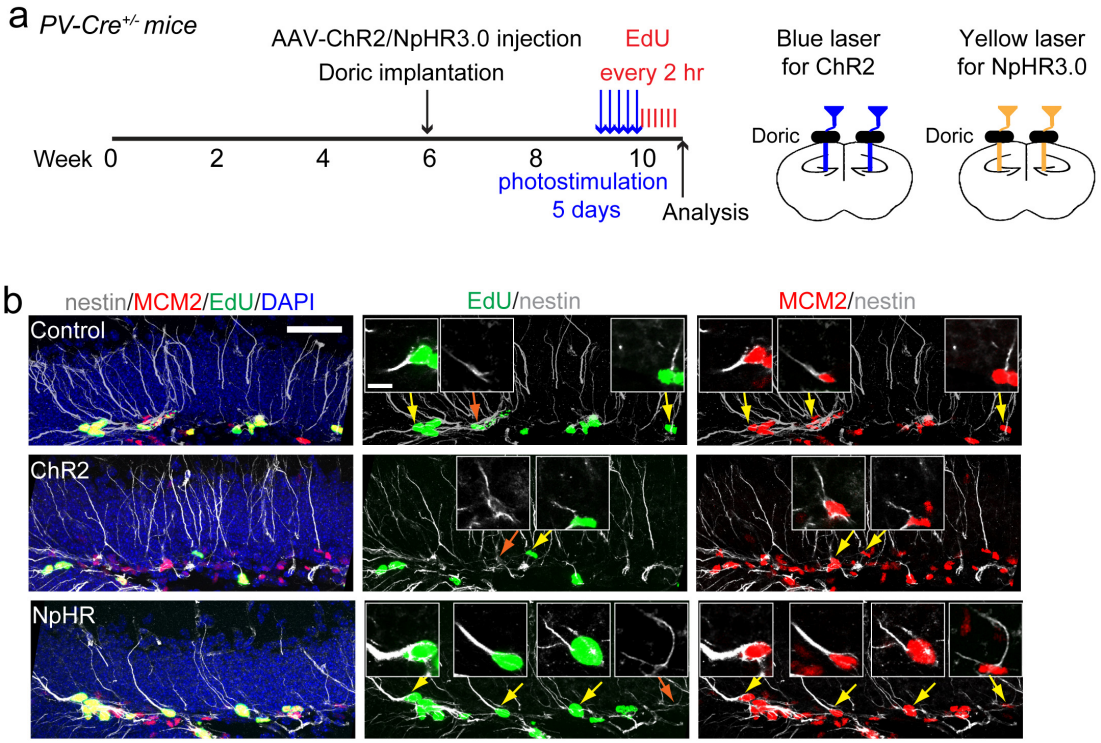

Supplementary Figure 5. Analysis of effects of *in vivo* manipulation of PV$^+$ interneuron activity on RGL activation in the adult dentate gyrus of *PV-Cre* mice. a, A schematic diagram of analysis of RGL activation at the population level upon photo-activation or photo-suppression of PV$^+$ interneurons in the dentate gyrus of adult *PV-Cre* mice (related to **Fig. 4d**). For photo-activation of PV$^+$ interneurons, blue light flashes (472 nm; 5 ms at 8 Hz) were delivered every 5 minutes for 30s/per trial, 8 hrs per day for 5 days. For photo-suppression of PV$^+$ interneurons, continuous yellow light (593 nm; constant) was delivered 8 hrs per day for 5 days. On the 5th day, animals were *i.p.* injected with EdU (41.1 mg/kg body weight) 6 times 2 hrs apart and processed for immunohistology 2 hrs after the last EdU injection. **b**, Sample confocal images of immunostaining of nestin (white), MCM2 (red), EdU (green) and DAPI (blue). Yellow arrows point to double labelled RGLs (nestin$^+$MCM2$^+$ or nestin$^+$EdU$^+$ cells with radial process) and orange arrows point to EdU$^-$ or MCM2$^-$ nextin$^+$ cells. Scale bars: 50 μm and 10 μm (insert).

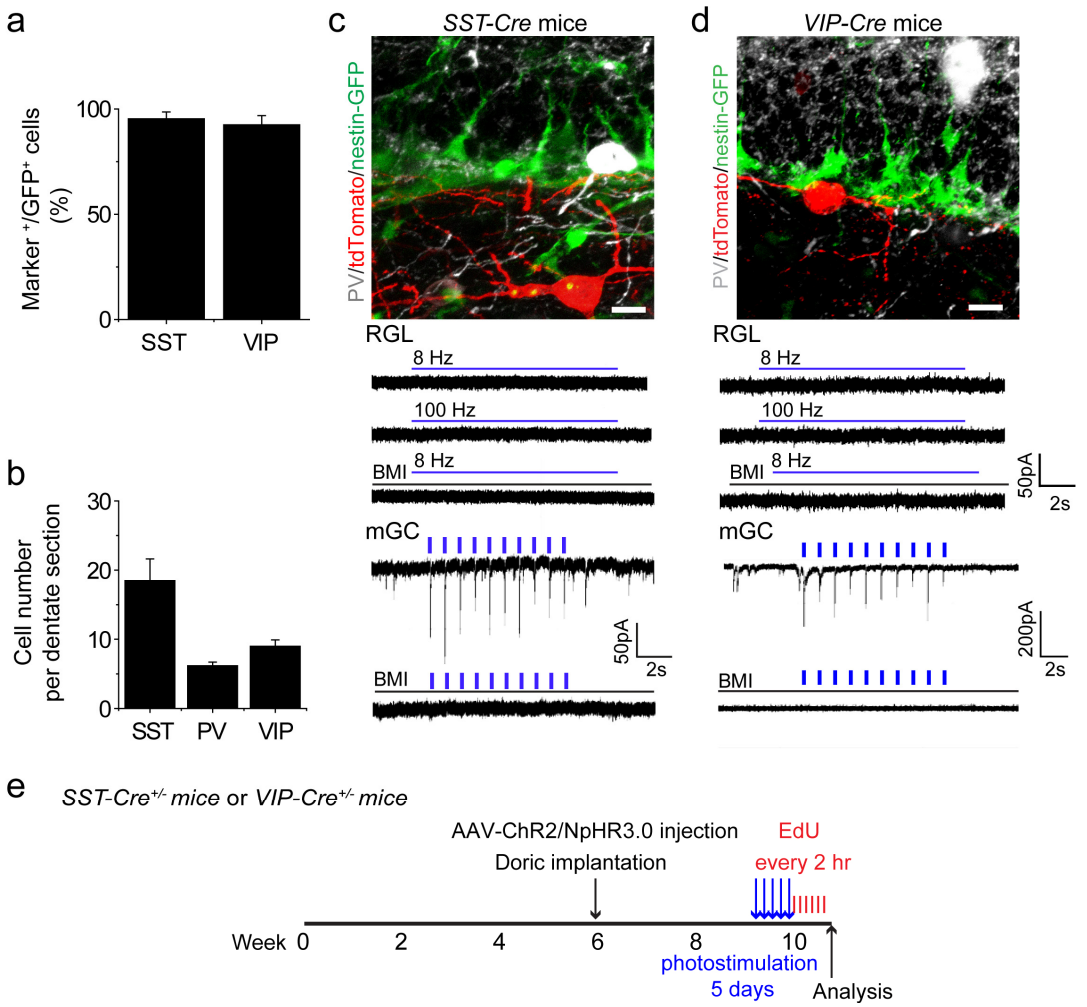

Supplementary Figure 6. Characterization of optogenetic tools for manipulating SST$^+$ and VIP$^+$ interneuron activity in the adult dentate gyrus. a-b, Characterization of opsin expression in different animal models. Shown in (**a**) is a quantification of immunohistological analysis of the specificity of ChR2 expression in SST$^+$ and VIP$^+$ interneurons after AAV-DIO-ChR2-YFP injection into the dentate gyrus of adult *SST-Cre* or *VIP-Cre* mice, respectively. Shown in (**b**) is a summary of quantification of numbers of ChR2-YFP labelled neurons after AAV-DIO-ChR2-YFP injection into the dentate gyrus of adult *PV-Cre*, *SST-Cre* or *VIP-Cre* mice. Values represent mean ± s.e.m. (n = 3-10 animals). **c**, Lack of responses of RGLs to SST$^+$ interneuron activation. Shown at the top is a sample confocal image of nestin-GFP, ChR2-tdTomato, and PV immunostaining in the dentate gyrus of adult *SST-Cre*$^{+/-}$*nestin-GFP*$^{+/-}$ mice after AAV-DIO-ChR2-tdTomato injection. Scale bar: 10 μm. Shown at the bottom are sample whole-cell voltage-clamp recording traces from a GFP$^+$ RGL upon light stimulation of SST$^+$ neurons (472 nm blue light at 8 or 100 Hz) and from a mature dentate granule cell (mGC; at 1 Hz) upon light stimulation of SST$^+$ interneurons in the acute slices before and after bicuculline treatment (BMI; 50 μM). **d**, Lack of responses of RGLs to VIP$^+$ interneuron activation. Similar as in (**c**), except adult *VIP-Cre*$^{+/-}$*nestin-GFP*$^{+/-}$ mice were used. **e**, A schematic diagram of analysis of RGL activation at the population level upon photo-activation or photo-suppression of SST$^+$ or VIP$^+$ interneurons in the adult dentate gyrus. The same paradigm as in Supplementary Fig. 5a was used.

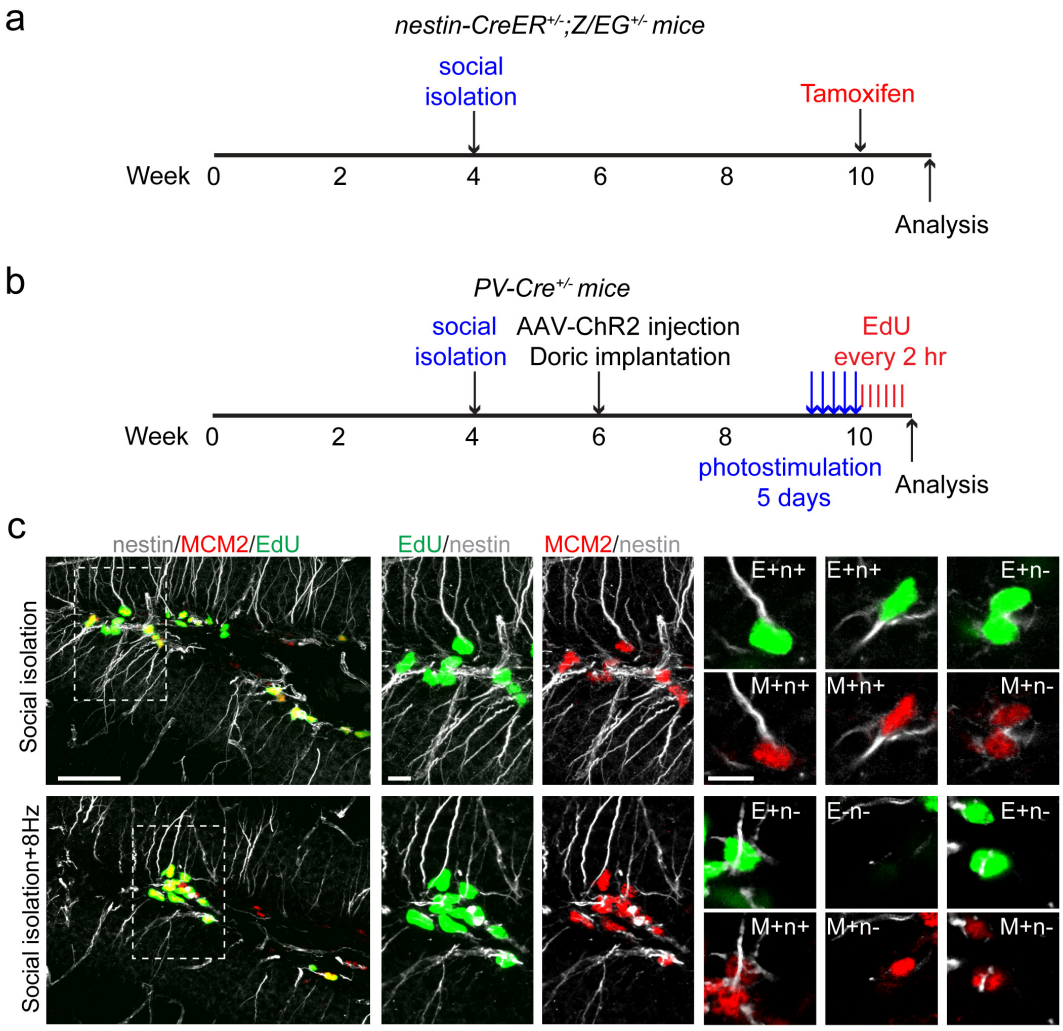

Supplementary Figure 7. Experimental schemes involving social isolation. a, A schematic diagram of clonal analysis of RGLs upon social isolation (related to **Fig. 5a-b**). **b**, A schematic diagram of analysis of RGL activation at the population level upon photo-stimulation of PV^+ interneurons in the adult dentate gyrus following social isolation (relate to **Fig. 5c**). Same paradigm of photo-stimulation and EdU injections as in Supplementary Fig. 5a was used. **c**, Sample confocal images of immunostaining for nestin (white; n), MCM2 (red; M), and EdU (green; E). Scale bars: 50 μm (left column) and 10 μm for inserts (five right columns).

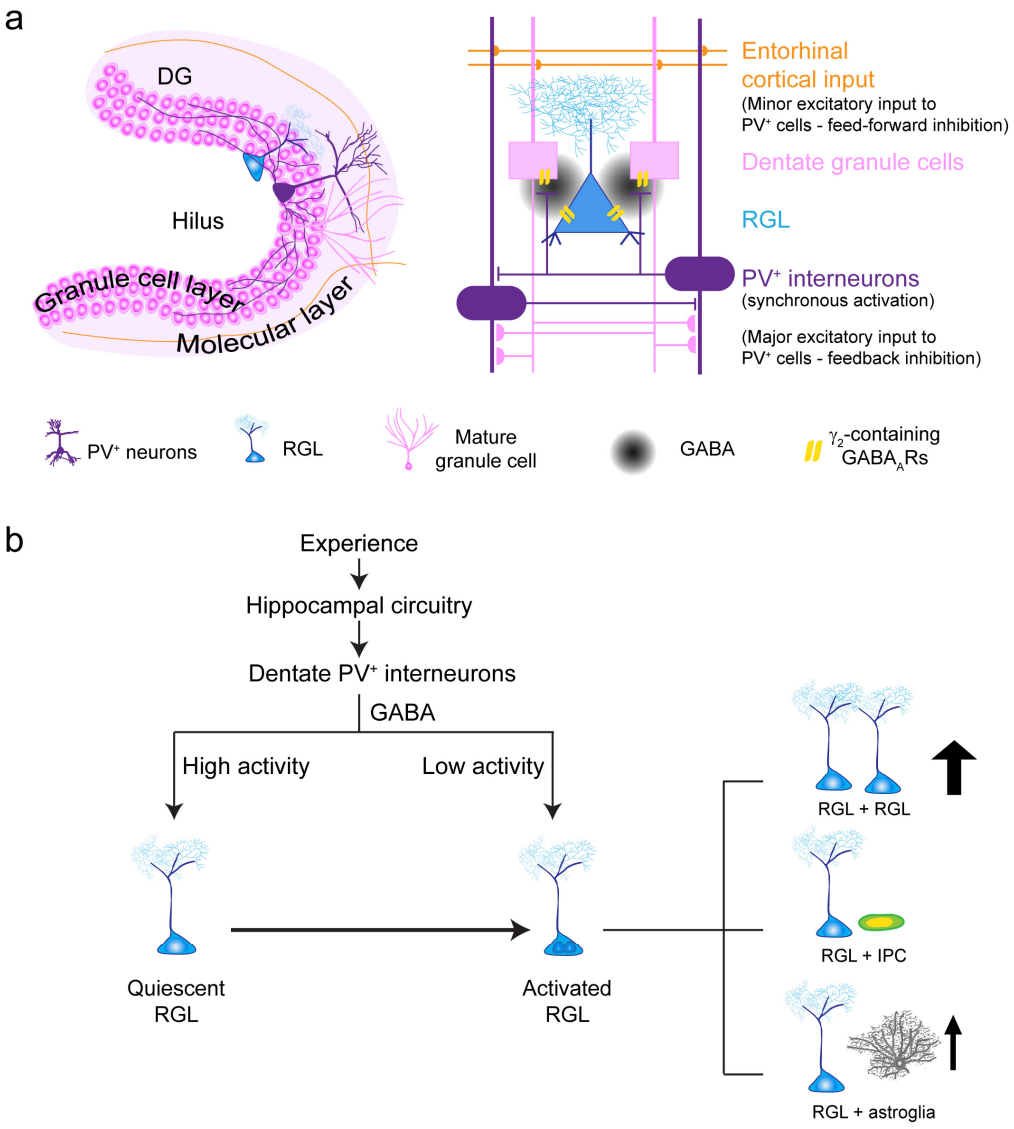

Supplementary Figure 8. A summary model of regulation of quiescent adult neural stem cells *in vivo* in response to neuronal activity and experience, involving GABA release from local PV$^+$ interneurons and γ_2-containing GABA$_A$R-mediated signalling in RGLs in the adult dentate gyrus. a, Schematic diagrams of local dentate gyrus circuitry. PV$^+$ interneurons receive excitatory inputs from both dentate granule cells (90%) and entorhinal cortical inputs (5%). PV$^+$ interneurons are also coupled with each other and fire synchronously. PV$^+$ interneurons innervate dentate granule cell layer and spillover of GABA from synaptic junctions regulates nearby radial glia-like neural stem cells (RGLs). **b**, A model of neuronal activity-dependent regulation of radial glia-like neural stem cell fate decision in the adult dentate gyrus. High levels of PV$^+$ interneuron activity promote quiescence of neural stem cells, whereas low levels of PV$^+$ interneuron activity promote activation of neural stem cells and symmetric cell division.

Supplementary Movies

Supplementary Movie 1. Close association between GFP$^+$ RGLs and GAD67$^+$ terminals of PV$^+$ interneurons in the adult dentate gyrus. Shown is a surface-rendered reconstruction of confocal images of the dentate gyrus (90 x 90 x 30 μm) of adult *nestin-GFP* mice for immunostaining of nestin-GFP (green), PV$^+$GAD67$^+$ (blue) and PV$^-$GAD67$^+$ (red).

Supplementary Movie 2. Lack of interaction between SST$^+$ interneurons and RGLs in the adult dentate gyrus. Shown is a surface-rendered reconstruction of confocal images of PV immunostaining (white), ChR2-tdTomato expression by SST$^+$ interneurons (red) and nestin-GFP expression in RGLs (green). DIO-ChR2-mCherry AAV was injected into *SST-Cre$^{+/-}$;nestin-GFP$^{+/-}$* mice and sections were processed for immunostaining two weeks later. Note that SST$^+$ interneurons extend neuronal processes in the subgranular zone and hilus region, whereas PV$^+$ interneurons exhibit elaborated processes in the subgranular zone and granule cell layer in the adult dentate gyrus.

Supplementary Movie 3. A single PV$^+$ interneuron has the capacity to regulate a large number of RGLs in the adult dentate gyrus. Shown is a surface reconstruction of serial confocal images of a single PV$^+$ interneuron in the adult dentate gyrus. A small volume of DIO-mCherry AAV was injected into *PV-Cre$^{+/-}$;nestin-GFP$^{+/-}$* mice and a region with a single PV$^+$ neuron was confocal imaged for mCherry (PV$^+$ neuron) and GFP (nestin-expressing cells) 2 weeks after injection and reconstructed from 8 serial coronal sections (50 μm in thickness oer section). An estimated 200+ GFP$^+$ RGLs were covered by a single PV$^+$ interneuron in the adult dentate gyrus.